ELSEVIER Nuclear Instruments and Methods in Physics Research B 164–165 (2000) 614–625

NIM B
Beam Interactions with Materials & Atoms

www.elsevier.nl/locate/nimb

Electron dynamics and level broadening in slow atomic interactions with metal surfaces and thin metallic films

B. Bahrim [a], P. Kürpick [a,1], U. Thumm [a,b], U. Wille [c,*]

[a] *J.R. Macdonald Laboratory, Department of Physics, Kansas State University, Manhattan, Kansas 66506-2601, USA*
[b] *Institute for Theoretical Atomic and Molecular Physics, Harvard-Smithsonian Center for Astrophysics, 60 Garden Street, Cambridge, MA 02138, USA*
[c] *Bereich Theoretische Physik, Hahn-Meitner-Institut Berlin, Glienicker Str. 100, D-14109 Berlin, Germany*

Abstract

Theoretical results on the electron dynamics and on resonant level broadening in slow atomic interactions with metal surfaces and thin metallic films are presented. Within the time-dependent close-coupling method, a wave-packet approach is introduced in which nondiagonal couplings in the subspace of metal states are taken into account. This approach is applied in a study of the time evolution of the occupation of hydrogen states in front of a semi-infinite metal. First-order level widths are calculated for hydrogenic atoms interacting with thin metallic films. They are found to exhibit pronounced size-quantization effects arising from the confinement of the electronic motion in the growth direction of the film.

PACS: 79.20.Rf; 34.50.Dy; 34.70.+e; 73.20.Dx

1. Introduction

Studies of interactions of *slow* atoms and ions with solid *surfaces*, in particular with *metal* surfaces, form a substantial part of the current research activities in the field of atom–solid interactions. In contrast to swift collisions in which the electron dynamics is governed by the kinetic energy of the atoms, electronic processes in slow atom–metal–surface collisions are driven by the potential energy carried into the interaction region by excited or ionized atomic particles [1,2]. In this case, resonant one-electron processes (resonance ionization, resonance neutralization) as well as Auger-type two-electron processes (Auger de-excitation, Auger neutralization) are responsible for charge transfer and electron emission. Over the past decades, a vast number of experimental and theoretical studies have dealt with various aspects of electronic processes in slow atom-surface interactions [3–11]. In recent years, particular emphasis has been placed on the investigation of surface interactions of highly charged ions [12]. Aside from their basic scientific relevance, studies

* Corresponding author. Tel.: +49-30-8062-2685; fax: +49-30-8062-2098.
E-mail address: wille@hmi.de (U. Wille).
[1] Present address: SAP, Neurottstr. 16, D-69190 Walldorf, Germany.

0168-583X/00/$ - see front matter
PII: S0168-583X(99)01158-1

of atom–surface interactions become increasingly important in conjunction with technological applications (see, e.g. Refs. [10,12], and pertinent papers in the present volume).

For the theoretical treatment of electronic processes in atom–metal–surface interactions, a variety of models and approaches based on the classical-trajectory approximation to the atomic motion have been devised and applied. Recently, particular interest has been devoted to the non-perturbative study of resonance formation of atomic systems in front of metal surfaces. Extensive calculations of (adiabatic) resonance energies and widths have been performed using the self-energy concept [13–15], the coupled-angular-mode (CAM) method [16–20], the complex-scaling approach [21–23], and the stabilization method [24–27]. Within the rate-equation approach, adiabatic energies and widths have been used in time-dependent calculations of resonance ionization of Rydberg atoms [28–30]. Fully quantal, time-dependent close-coupling calculations based on an expansion of the total one-electron wave function in terms of adiabatic resonance states [14,15] have been initiated [31]. For the description of surface interactions of highly charged ions, in which multi-electron transfer takes place into ionic states with high principal quantum numbers, "over-barrier" models describing electron transfer as well as the subsequent de-excitation and emission processes in terms of classical electron currents and rate equations have been introduced [32–35]. In contrast to interactions with surfaces of semi-infinite metals, atomic interactions with thin metallic films have so far remained a largely unexplored topic [36,37].

In the present paper, we discuss new theoretical results on atomic interactions with metal surfaces and thin metallic films. Within the time-dependent close-coupling method, we apply a novel wave-packet approach in which nondiagonal couplings in the subspace of metal states, i.e., (direct) inelastic transitions within the conduction band, are taken into account (Section 3). This feature distinguishes our approach from the time-dependent optical-model approach [38] and the (fixed-atom) self-energy method [13–15]. For atoms interacting with thin metallic films, we study size-quantization effects in resonant level broadening by calculating first-order level widths as a function of film thickness (Section 4). In order to put the present results into proper perspective, we outline and illustrate in Section 2 the general framework underlying the time-dependent description of atom–surface interactions. Throughout this paper, we use atomic units ($e = m_e = \hbar = 1$).

2. General framework

Adopting a reference frame in which the metal is at rest, we describe the atomic motion in front of the surface in terms of prescribed classical trajectories $\vec{D}(t)$. The electron dynamics in the atom–metal system is then determined by a time-dependent Hamiltonian $H(t) \equiv H(\vec{D}(t))$. The total wave function $\Psi(\vec{r};t)$ for a single active electron or hole with position vector $\vec{r}$ obeys the one-particle Schrödinger equation

$$H(t)\Psi(\vec{r};t) = \mathrm{i}\dot{\Psi}(\vec{r};t) \tag{1}$$

(coordinates $\vec{r} \equiv (x,y,z)$ are used such that the (x,y)-plane coincides with the jellium edge of the metal and the z-axis points towards the vaccum). The function $\Psi(\vec{r};t)$ is expanded as

$$\Psi(\vec{r};t) = \sum_j a_j(t)\psi_j(\vec{r};t)\mathrm{e}^{-\mathrm{i}\epsilon_j t} + \int \mathrm{d}\vec{k}\rho(\vec{k})\, b_{\vec{k}}(t)\phi_{\vec{k}}(\vec{r})\mathrm{e}^{-\mathrm{i}\epsilon_{\vec{k}} t}, \quad j = 1,\ldots,N; \quad k \leqslant k_{\max}, \tag{2}$$

where the basis functions $\psi_j(\vec{r};t) \equiv \psi_j(\vec{r};\vec{D}(t))$ are bound-state atomic wave functions with energies ϵ_j, centered at the site of the atom (the label j denotes collectively a set of single-particle quantum numbers; translational factors are neglected). The basis functions $\phi_{\vec{k}}(\vec{r})$ are jellium-type metal wave functions corresponding to wave vector $\vec{k}$ and energy $\epsilon_{\vec{k}}$, and $\rho(\vec{k})$ is the density of states. Channel decompositions of the total Hamiltonian $H(t)$ are introduced by writing

$$H(t) = H_i + V_i(t) = H_f(t) + V_f(t), \tag{3}$$

where the Hamiltonian $H_i(H_f)$ defines the unperturbed jellium states (atomic states), and $V_i(V_f)$ is

the initial-channel (final-channel) perturbation (we adopt the convention that the active electron or hole *initially* occupies a jellium state).

By inserting expansion (2) into Eq. (1) and projecting onto the basis functions, one obtains a system of coupled integrodifferential equations [38] for the amplitudes $a_j(t)$ and $b_{\vec{k}}(t)$, which is virtually intractable. In the optical-model approach [38], one remedies this situation by disregarding the nondiagonal couplings among the jellium states, so that the amplitudes $b_{\vec{k}}(t)$ can be eliminated from the set of close-coupling equations. The resulting system of equations for the amplitudes $a_j(t)$ involves a complex potential matrix ("optical potential") which is nonlocal in time. In the fixed-atom limit, where the atom is at rest at a distance D in front of the surface, the Hamiltonian H, and consequently the optical potential, do not explicitly depend upon time. The optical potential then determines the (adiabatic) resonance states formed at fixed D. Using instead of the optical potential the closely related self-energy matrix $\mathcal{S}$ [13,14] and invoking the Wigner–Weisskopf approximation [13,39,14], one obtains the (real) energies E_μ and the widths Γ_μ of the resonance states from the complex eigenvalues ω_μ of $\mathcal{S}$ as

$$E_\mu = \mathrm{Re}\ \omega_\mu, \quad \Gamma_\mu = -2\ \mathrm{Im}\ \omega_\mu. \tag{4}$$

The associated eigenvectors represent the atomic-subspace projections χ_μ of the resonance wavefunctions.

Using the self-energy method, we have performed large-scale calculations of resonance energies and widths [14,15] for the case of a semi-infinite metal. The channel Hamiltonians H_i and H_f have been defined in terms of a step-like jellium potential and the pure Coulomb potential (with effective core charge Z), respectively, and classical image potentials have been assumed in the construction of the channel perturbations V_i and V_f. The numerical calculations rely crucially on the efficient evaluation of coupling and overlap matrix elements using the analytical techniques developed in Refs. [40,41].

For the purpose of illustration, energies of the $m = 0$ resonance states emerging from the asymptotic $n = 5$ to $n = 7$ manifolds for core charge $Z = 3$ near an Al surface [15] are shown in Fig. 1(a) as a function of ion-surface distance D. Our calculation has been performed within the basis set spanned by the $n = 3$ to $n = 9$ manifolds. For comparison, results for the $n = 5, m = 0$ manifold obtained by Borisov et al. [20] using the nonperturbative CAM method are also shown. The discrepancies between the CAM results and our self-energy calculations originate mainly from our approximation of the core image potential, which leads to somewhat larger upward shifts of all levels.

In Fig. 1(b), level widths of those resonance states in Fig. 1(a) that merge in the asymptotic

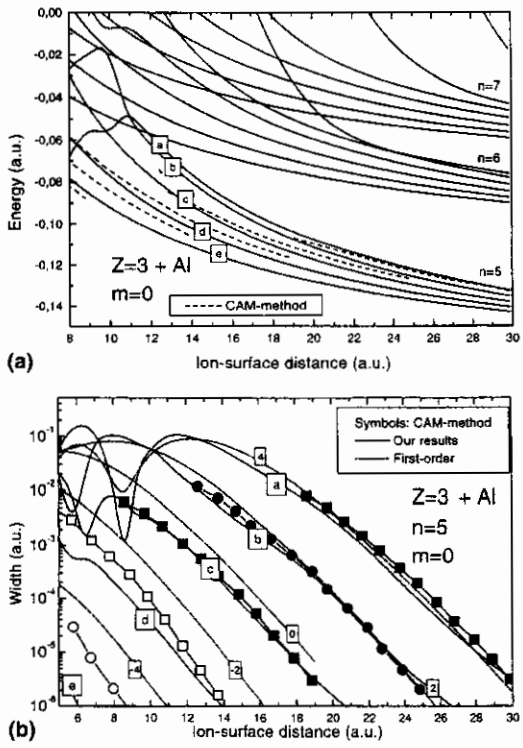

Fig. 1. (a) Energies of the $m = 0$ resonance states emerging from the asymptotic $n = 5$ to $n = 7$ manifolds for core charge $Z = 3$ near an Al surface [15]. The dashed lines show results of the CAM method [20] for the $n = 5, m = 0$ manifold. (b) Widths of the $n = 5, m = 0$ resonance states for core charge $Z = 3$ near an Al surface [15]. The symbols show results of the CAM method [18,19]. The dash-dotted lines labelled by the electric quantum number k are results of first-order calculations in the parabolic (Stark) basis [18,19]. The labels [a] to [e] in part (a) and (b), respectively, refer to one and the same resonance state.

$n = 5$ manifold of the $Z = 3$ hydrogenic ion [15] are shown as a function of ion–surface distance D. The symbols refer to the nonperturbative CAM calculation of Ref. [18,19]. Although this calculation uses the refined surface potential of Jennings et al. [42], our widths tend to agree very well with the CAM results for the three states exhibiting the largest widths (for details, see Ref. [15]). In Fig. 1(b), we have also plotted first-order widths for parabolic (Stark) states [18,19], obtained with the surface potential used in our self-energy calculations. For the Stark states with the largest widths, there is good agreement between first-order and nonperturbative results, while for the other states the first-order widths are considerably larger than the nonperturbative widths.

In our calculations [14,15], we have obtained converged results for resonance energies and widths as well as for the associated wavefunctions over broad ranges of the atom–surface distance and of the atomic quantum numbers. Therefore, the self-energy method appears to be well suited for the generation of surface resonance states as "two-center" basis functions for the solution of the time-dependent Schrödinger equation, in close analogy to the quasimolecular treatment of slow ion–atom collisions [43]. In order to exemplify this aspect, we have initiated time-dependent calculations for ionization of highly excited atoms, using a basis of adiabatic resonance states χ_μ obtained by diagonalizing the self-energy matrix $\mathcal{S}$ [31].

With the wave function $\Psi(\vec{r};t)$ expanded as

$$\Psi(\vec{r};t) = \sum_{\mu=1}^{\Lambda} c_\mu(t)\chi_\mu(\vec{r};D(t)) \times \exp\left[-\mathrm{i}\int^{t} \mathrm{d}t' E_\mu(D(t'))\right], \tag{5}$$

the coupled equations for the occupation amplitudes $c_\mu(t)$ are obtained as

$$\dot{c}_\mu(t) = -\sum_{\mu'=1}^{\Lambda} c_{\mu'}(t)\left\langle \chi_\mu(D(t))\left|\frac{\partial}{\partial t} + \frac{\Gamma_\mu}{2}\delta_{\mu\mu'}\right|\chi_{\mu'}(D(t))\right\rangle \times \exp\left[-\mathrm{i}\int^{t} \mathrm{d}t'\{E_{\mu'}(D(t')) - E_\mu(D(t'))\}\right]. \tag{6}$$

The operator $\partial/\partial t \equiv -v_z\partial/\partial D$ (for perpendicular incidence of the atom at constant velocity v_z) gives rise to velocity-dependent off-diagonal couplings ("dynamic couplings" [43]) between the resonance states $\chi_\mu(D)$. The diagonal width term $\Gamma_\mu/2$ describes the decay (induced by the potential couplings between the atom and metal subspaces) of the resonance state $\chi_\mu(D)$ with energy above the Fermi level of the metal into empty jellium states. By suppressing the dynamic couplings in Eqs. (6), we retrieve the classical rate equations used by Nordlander et al. [28–30]. In order to simulate the conditions of current experiments [44,45], we have included in our calculations the effect of a uniform (external) electric field of strength F. Total probabilities for the statistically populated hydrogen $n = 5, m = 0$ manifold to become ionized when the atom approaches an Al surface down to atom–surface distance D, calculated from the solution of Eqs. (6), are shown in Fig. 2 for two perpendicular velocities v_z and two field strengths F, both with the dynamic couplings disregarded and with the dynamic couplings fully included.

The external electric field is seen to have a very small effect only, except for atom–surface distances below 40 a.u. at $v_z = 2 \times 10^{-5}$ a.u. and below 30 a.u. at $v_z = 2 \times 10^{-2}$ a.u. When the velocity is raised from the lower value (which is roughly

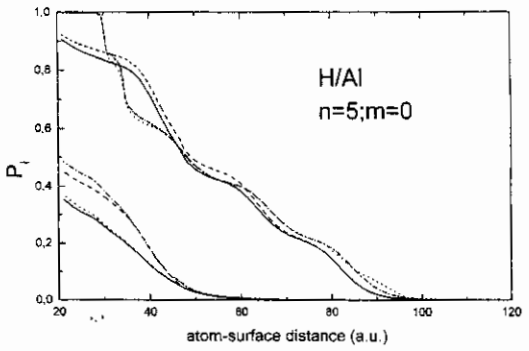

Fig. 2. Total probability for the statistically populated hydrogen $n = 5, m = 0$ manifold to become ionized when the atom approaches an Al surface down to atom–surface distance D [31]. Upper bunch of curves: $v_z = 2 \times 10^{-5}$ a.u.; lower bunch of curves: $v_z = 2 \times 10^{-2}$ a.u. Solid lines: no dynamic couplings, $F = 0$; dashed lines: dynamic couplings included, $F = 0$; dotted lines: no dynamic couplings, $F = 2.5 \times 10^{-5}$ a.u.; dash-dotted lines: dynamic couplings included, $F = 2.5 \times 10^{-5}$ a.u.

equal to the subthermal perpendicular velocity in the experiment of Ref. [44]) to the higher value, the ion production sets in at much shorter distances and tends to be smaller throughout. This feature is related to the smaller time available for the decay of the resonance states (mediated by the width terms Γ_μ in Eqs. (6)) when the atom approaches the surface with higher velocity. The effect of the dynamic couplings is very small at $v_z = 2 \times 10^{-5}$ a.u. Hence, we may conclude that the classical rate-equation approach is justified for subthermal and thermal velocities. At $v_z = 2 \times 10^{-2}$ a.u., however, the dynamic couplings influence the ion production significantly, so that a fully time-dependent, quantal treatment is appropriate.

3. Wave-packet approach

In our wave-packet approach [46], we discretize the continuum of metal states by replacing it with a finite number M of normalizable wave packets ("Weyl packets" [47]), each formed by superimposing jellium functions within a narrow wave-number interval. Using these wave packets in the expansion of the wave function $\Psi(\vec{r};t)$ (cf. Eq. (2)), we obtain $N+M$ coupled differential equations, in which the nondiagonal couplings within the metal subspace are fully taken into account. This feature distinguishes the wave-packet approach from the optical-model approach, in which different metal states can interact only indirectly via the atomic states.

Adopting a step-like jellium potential with depth V_0 inside the metal, we construct wave packets $\phi_n(z)$ describing the electronic motion in the z-direction by superimposing jellium wave functions $\phi_{k_z}(z)$ in k_z-intervals (labeled $n = 1,2,\ldots$) with centroid wave number $k_n \equiv k_z^{(n)}$ and constant length δ_z:

$$\phi_n(z) = \sqrt{\frac{\delta_z}{2\pi}}\left\{\frac{2\sin(\delta_z z/2)}{\delta_z z}[e^{ik_n z} + R_n e^{-ik_n z}]\theta(-z) + T_n e^{-\gamma_n z}\theta(z)\right\}, \tag{7}$$

where $\gamma_n = \sqrt{2V_0 - k_n^2}$, and R_n and T_n are the reflection coefficient and transmission coefficient, respectively, for centroid wave number k_n. For the motion in the surface plane ((x,y)-plane), wave packets $\phi_l(x)$ and $\phi_m(y)$ are obtained by superimposing plane waves with wave number component k_x and k_y in intervals (labeled $l = 1,2,\ldots$ and $m = 1,2,\ldots$) with centroid $k_l \equiv k_x^{(l)}$ and $k_m \equiv k_y^{(m)}$ and length δ_x and δ_y, respectively,

$$\phi_l(x) = \sqrt{\frac{\delta_x}{2\pi}}\frac{2\sin(\delta_x x/2)}{\delta_x x}e^{ik_l x}, \tag{8a}$$

$$\phi_m(y) = \sqrt{\frac{\delta_y}{2\pi}}\frac{2\sin(\delta_y y/2)}{\delta_y y}e^{ik_m y}. \tag{8b}$$

The "metal part" of the total wave function $\Psi(\vec{r};t)$ (second term in the right-hand side of Eq. (2)) can now be approximated as

$$\int d\vec{k}\rho(\vec{k})b_{\vec{k}}(t)\phi_{\vec{k}}(\vec{r})e^{-i\epsilon_{\vec{k}}t} \approx \sum_\alpha b_\alpha(t)\phi_\alpha(\vec{r})e^{-i\epsilon_\alpha t}, \tag{9}$$

where

$$\phi_\alpha(\vec{r}) = \phi_l(x)\phi_m(y)\phi_n(z), \tag{10}$$

and

$$\epsilon_\alpha = \frac{k_l^2}{2} + \frac{k_m^2}{2} + \frac{k_n^2}{2} - V_0, \tag{11}$$

with $\alpha = (l,m,n)$ and $l+m+n \leqslant M$. The functions $\phi_\alpha(\vec{r})$ are (with respect to integration over the full $\vec{r}$-space) orthogonal and normalized to unity.

Insertion into Eq. (1) of the expansion (2) with the metal part (9) leads to the system of coupled equations

$$i\begin{pmatrix} 1 & \vdots & \langle\psi_j|\phi_\alpha\rangle \\ \cdots & \cdot & \cdots \\ \langle\phi_\alpha|\psi_j\rangle & \vdots & 1 \end{pmatrix}\begin{pmatrix} e^{-i\epsilon_l t} & \vdots & 0 \\ \cdots & \cdot & \cdots \\ 0 & \vdots & e^{-i\epsilon_\alpha t} \end{pmatrix}\begin{pmatrix} \dot{a}_j(t) \\ \cdot \\ \dot{b}_\alpha(t) \end{pmatrix} = \begin{pmatrix} \langle\psi_{j'}|V_f|\psi_{j'}\rangle & \vdots & \langle\psi_j|V_i|\phi_{\alpha'}\rangle \\ \cdots & \cdot & \cdots \\ \langle\phi_\alpha|V_i|\psi_j\rangle & \vdots & \langle\phi_\alpha|V_i|\phi_{\alpha'}\rangle \end{pmatrix} \times \begin{pmatrix} e^{-i\epsilon_{j'}t} & \vdots & 0 \\ \cdots & \cdot & \cdots \\ 0 & \vdots & e^{-i\epsilon_{\alpha'}t} \end{pmatrix}\begin{pmatrix} a_{j'}(t) \\ \cdot \\ b_{\alpha'}(t) \end{pmatrix}. \tag{12}$$

The matrix elements $\langle\phi_\alpha|V_i|\phi_{\alpha'}\rangle$ describe the direct couplings between the wave packets. By

numerically solving Eqs. (12) for a given initial occupation, we obtain the atomic and metal occupation amplitudes $a_j(t)$ and $b_\alpha(t)$ as a function of time.

In order to demonstrate the feasibility of our wave-packet approach, we consider the case of perpendicular incidence of 2p ($m = 0$) hydrogen atoms with velocity $v_z = 5 \times 10^{-3}$ a.u. upon an Al surface. In the atomic subspace, we include all states with $n \leqslant 5$ and $m = 0$ (as the magnetic quantum number m is a conserved quantity, only $m = 0$ states couple to the initial state). With this choice, our results for the $n = 2$ manifold are converged with respect to the atomic basis size. The metal subspace is spanned by 160 wave-packets ϕ_n describing the electronic motion in the z-direction. For this number of wave packets, our results are converged to respect to the size of the z-dependent part of the metal subspace. For ease of calculation, we confine the motion of the active electron in the surface plane by choosing a single wave packet, in which only in-plane wave numbers $k_\parallel \equiv \sqrt{k_x^2 + k_y^2} \leqslant 0.02$ a.u. are taken into account (in this range, the relevant transition matrix elements can be approximated by their value at $k_\parallel = 0$). We calculate the time evolution of the system along a (reflected) straight-line trajectory with distance of closest approach $D_{\min} = 3.5$ a.u. determined from a planar-averaged Thomas–Fermi–Molière potential [34].

In Fig. 3, occupation probabilities of the $n = 2, m = 0$ and $n = 3, m = 0$ atomic manifolds as well as the sum of the probabilities of all 160 metal states are shown as a function of the atom–surface distance D. On the incoming branch of the atomic trajectory, for distances larger than about 18 a.u., only Stark-like mixing between the 2s and 2p ($m = 0$) states occurs. At $D \approx 18$ a.u., population of the $n = 3$ manifold (thin lines in Fig. 3) sets in at the expense of the population of the initially occupied 2p ($m = 0$) states, thereby suppressing the mixing of the 2s and 2p ($m = 0$) states. Electron transfer to the metal starts at $D \approx 12$ a.u., i.e., at a distance lying between the classical threshold dis-

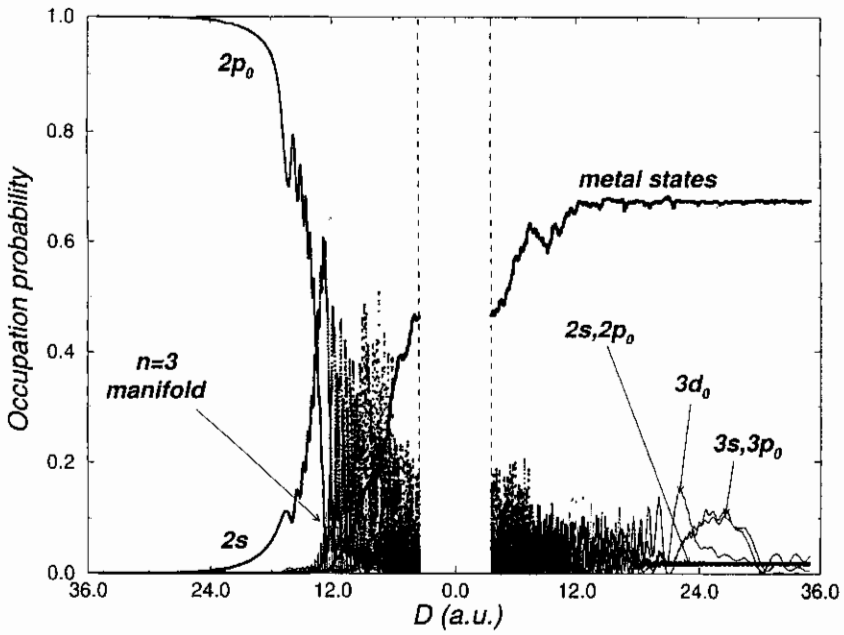

Fig. 3. Occupation probabilities of the atomic $n = 2, m = 0$ and $n = 3, m = 0$ manifolds and of the metal states for perpendicular incidence of 2p ($m = 0$) hydrogen atoms with velocity $v_z = 5 \times 10^{-3}$ a.u. upon an Al surface, plotted as a function of atom–surface distance D for the incoming branch (left part) and the outgoing branch (right part) of the atomic trajectory. For further explanation, see text.

tances $D_{n=2} = 8$ a.u. and $D_{n=3} = 18$ a.u. On the outgoing branch of the trajectory, the occupation of the $n = 2$ states tends to stabilize for $D > 20$ a.u., while Stark-like mixing among the $n = 3$ states as well as interactions with other atomic states continue to change the occupations in the $n = 3, m = 0$ subspace. The occupation of the metal states stabilizes beyond $D \approx 12$ a.u., i.e., beyond the distance where electron transfer to the metal sets in on the incoming branch.

In Fig. 4, the results of Fig. 3 are shown in parabolic representation, in which hydrogenic orbitals are described in terms of the quantum numbers n, k, m, instead of the quantum numbers n, l, m of the spherical representation. The quantum number k is the "electric" quantum number. A comparison of Figs. 3 and 4 shows that the parabolic basis is more appropriate to describe the interaction at large distances, where the perturbing field of the surface changes relatively little over the extent of the projectile orbits and thus leads to the hybridization of spherical hydrogenic states into "Stark-like" states labelled n, k, m [15]. Accordingly, we find that for the $n = 2$ manifold, the population of the parabolic states with electric quantum numbers $k = -1$ and $+1$ varies less than the $2s$ and $2p_0$ population in Fig. 3. The $k = 1$ state is oriented towards the surface and couples stronger with the metal subspace (resulting in faster charge transfer) than the $k = -1$ state which is oriented away from surface. After the collision, the $k = 1$ component has become depopulated while the $k = -1$ component ends up with a (small) nonzero population.

4. Thin metallic films

The interaction of atoms and ions with thin metallic films is a topic that has attracted attention only recently [36,37]. Basically, one expects novel phenomena to occur in this type of interaction due to the confinement of the electronic motion in the growth direction of the film and to the associated quantization of the energy spectrum ("size quantization"), in much the same way as in the case of semiconductor quantum-well structures [48].

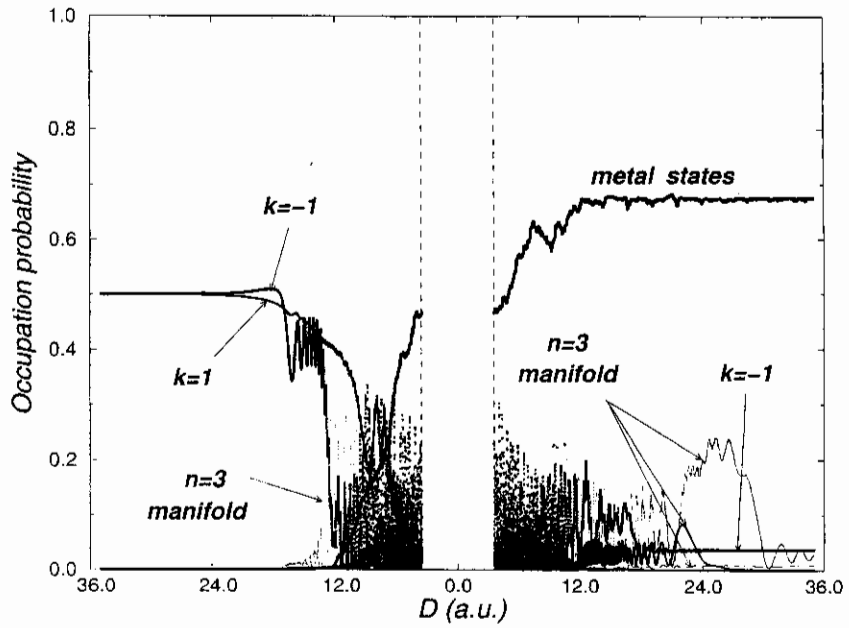

Fig. 4. Same as Fig. 3, but in parabolic representation for the hydrogen states. Electric quantum numbers $k = -1$ and $k = 1$ correspond to orbitals oriented away from and towards the surface.

We have studied the resonance broadening of hydrogenic levels near a thin metallic film by calculating first-order level widths (or, in other words, first-order rates for resonant transitions of electrons or holes between atom and film). While the nonperturbative self-energy method can be easily extended so as to be applicable to the case of metallic films, a first-order calculation of level widths (i.e., of the imaginary parts of the diagonal elements of the self-energy matrix) appears to be well suited to reveal the important novel features of the atom–film interaction.

For a jellium film of thickness L, we construct the unperturbed electronic potential $V_{\text{film}}(z)$ by employing the Jennings potential [42] (with one and the same set of parameters) to describe the interfaces on either side of the film [36,37]. With $z = 0$ at the midpoint of the film, the electronic potential reads

$$V_{\text{film}}(z) = \begin{cases} -V_0/\{A\exp[B(|z| - L/2)] + 1\}, & |z| \leqslant L/2 \\ -\{1 - \exp[-\eta(|z| - L/2)]\}/[4(|z| - L/2)], & |z| > L/2 \end{cases} \tag{13}$$

where $A = 4V_0/\eta - 1$, and $B = 2V_0/A$. For $|z| \to \infty$, this potential merges in the classical self-image potential of the electron. The total electronic wave functions of the film are written as

$$\phi_{\vec{k}_\parallel i}(\vec{r}) = \exp(\mathrm{i}\vec{k}_\parallel \cdot \vec{r}_\parallel)\phi_i(z), \tag{14}$$

where $\vec{k}_\parallel$ and $\vec{r}_\parallel$ are the components of wave vector and position vector, respectively, in the film plane. The functions $\phi_i(z)$ (with labels $i = 1, 2, \ldots$ arranged in order of increasing energy eigenvalue ϵ_i) are the bound-state eigenfunctions of the z-dependent part of the film Hamiltonian. The energies associated with the states $\phi_{\vec{k}_\parallel i}$ are given by

$$\epsilon_{k_\parallel i} = \frac{1}{2}k_\parallel^2 + \epsilon_i. \tag{15}$$

In Fig. 5, the dependence of the energies ϵ_i on the film thickness L for a thin Al(1 1 1) film is shown over an L-range corresponding approximately to a range of 2–14 monolayers.

The hydrogenic states of the unperturbed atomic system are described in terms of wave

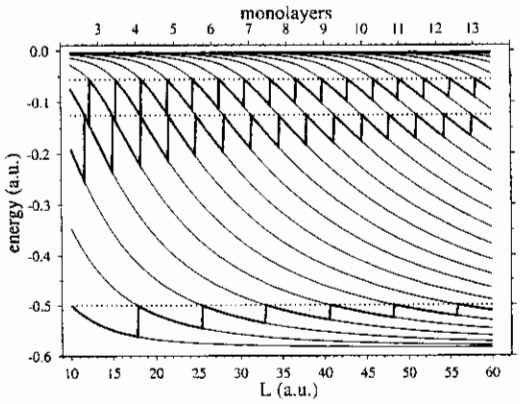

Fig. 5. Energy levels of a thin Al(1 1 1) film described by the potential (13) plotted as a function of film thickness L. The dotted horizontal lines indicate the unperturbed levels of the hydrogen atom for $n = 1, 2, 3$. The heavy solid lines emphasize those pieces of the film level curves that belong to the first film level *below* a given hydrogen level.

functions $\psi_{nkm}(\vec{r})$ in the parabolic (Stark) representation, in which the hybridization of the atomic orbitals induced by the long-range image charge interactions in the atom–metal system are, to some extent, taken into account [18,19,49]. The first-order width $\Gamma_{nkm}(D)$ of a level with quantum numbers n, k, m, associated with an atom located at a distance D from the adjacent jellium edge of the metallic film, is given by

$$\Gamma_{nkm}(D) = 2\pi\sum_i \int \mathrm{d}\vec{k}_\parallel \rho(\vec{k}_\parallel)|W_{nkm,\vec{k}_\parallel i}(D)|^2\delta(\epsilon_n - \epsilon_{k_\parallel i}) \equiv \sum_i |W_{nkm,k_\parallel^{(i)}}(D)|^2\Theta(\epsilon_n - \epsilon_i), \tag{16}$$

where $k_\parallel^{(i)} = \sqrt{2(\epsilon_n - \epsilon_i)}$, and $\epsilon_n = -Z^2/2n^2$ is the unperturbed energy of the hydrogenic level (we have disregarded here the lowest-order level shift $(2Z - 1)/4D$). The transition matrix element is written as

$$W_{nkm,\vec{k}_\parallel i}(D) = \langle\psi_{nkm}(D)|V_C^>(D)|\phi_{\vec{k}_\parallel i}\rangle, \tag{17}$$

where the perturbing potential $V_C^>$ is the Coulomb potential of the atomic core, cut-off at the "free" surface of the film at $z = L/2$ [50]. We have neglected the core *image* potential in the potentials defining the unperturbed atomic and film states as well as in the perturbing potential in Eq. (17). However, through the use of hydrogenic wave

functions in parabolic representation, its effect is partly taken into account in the atomic states.

In the form (16) the level width appears as a sum over a finite number of terms, each corresponding to the transition of an electron or hole (depending on the position of the atomic level ϵ_n relative to the (L-dependent) Fermi level ϵ_F of the film) into a film state with energy $\epsilon_i \leqslant \epsilon_n$ in the growth direction and (real) wave vector $k_\parallel^{(i)}$ of the free in-plane motion, such that the resonance condition $\epsilon_{k_\parallel i} = \epsilon_n$ is fulfilled.

In Fig. 6, the level widths $\Gamma_{nkm}(D)$ for a hydrogen atom ($Z = 1$) located at distances $D = 2n^2$ (these D-values are equal to the threshold distances for classical transitions [50]) in front of an Al(1 1 1) film are displayed as a function of film thickness L for $m = 0$ and $n = 1, 2$. The curves in the diagrams of the upper part of Fig. 6 exhibit the saw-tooth-like "gross structure" in the L-dependence, which arises from the thresholds for transitions into film levels (cf. Eq. (16)) at the L-values L_i where the film level curves ϵ_i in Fig. 5 intersect the horizontal line for a given atomic level ϵ_n and which, therefore, directly reflects the quantization of the film level spectrum in the z-direction. We have generated the gross structure curves by using the calculated widths only in the immediate vicinity of the points L_i, and by smoothly interpolating the curves (on a log-lin plot) between these points. The gross structure curves are in obvious correspondence to the saw-tooth patterns in Fig. 5, which were constructed by emphasizing those pieces of the film level curves that belong to the *first* level below a given atomic level.

In the intervals between adjacent points L_i, the actually calculated L-dependence of the level widths is found to exhibit (except for the atomic state with the largest value, $k_{max} = n - 1$, of the quantum number k within each n-manifold) detailed structure showing maxima and minima, as exemplified by the case $(n, k) = (2, -1)$ in the lower part of Fig. 6. This structure is related to the

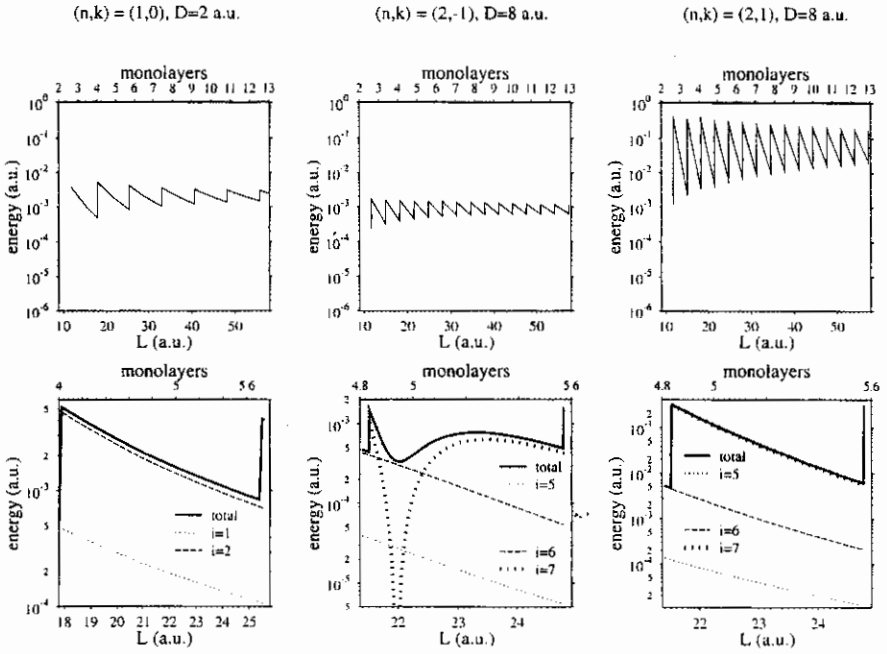

Fig. 6. Upper part: Gross structure of the L-dependence of the level widths Γ_{nkm} for a hydrogen atom located at the distances $D_n = 2n^2$ in front of an Al(1 1 1) film, for $m = 0$ and the indicated values of the quantum numbers n, k. Lower part: Detailed structure of the L-dependence of the level widths for selected L-intervals. Also shown are the contributions to the widths from the film states i lying energetically closest below the atomic level (cf. Fig. 5).

nodal structure of the atomic wave functions and can be shown [51] to image the dependence of the corresponding transitions matrix elements on the wave vector component $k_{\|}$ parallel to the surface in the case of a semi-infinite metal.

Assuming the atom to approach the film along a straight-line trajectory (with constant perpendicular velocity v_z), we can calculate atomic occupation probabilities $P_{nkm}(D)$ from the level widths $\Gamma_{nkm}(D)$ according to

$$P_{nkm}(D) = \exp\left\{-\frac{1}{v_z}\int_D^\infty \mathrm{d}D'\Gamma_{nkm}(D')\right\}. \qquad (18)$$

Transition distances D_{nkm} can be determined from the occupation probabilities by solving the equation $P_{nkm}(D_{nkm}) = 0.5$ (provided the probability drops from unity to zero in a sufficiently narrow D-range).

In Fig. 7, the detailed structure of the L-dependence of the transition distances for $v_z = 10^{-4}$ a.u. in the L-intervals of Fig. 6 is shown in a linear plot. The shapes of the curves closely resemble those of the level-width curves displayed (in a log-lin plot) in the lower part of Fig. 6. The reason behind this is the near-exponential behavior of the widths in the relevant D-range and the weak dependence of their slopes on L. The important feature revealed by Fig. 7 is the appearance of large threshold discontinuities in the transition distances, in particular for $(n,k) = (2,1)$. In general, the discontinuities for $k = k_{\max}$ are found to scale approximately as n^2, with their absolute values being close to $2n^2$, i.e., close to twice the atomic orbital radius or to the classical threshold distance D_n.

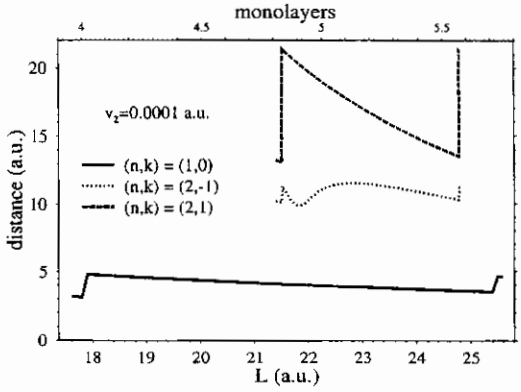

Fig. 7. Detailed structure of the L-dependence of the transition distances D_{nkm} for the examples of Fig. 6 and $v_z = 10^{-4}$ a.u.

The large threshold discontinuities in the dependence of the transition distances on the film thickness, as they are predicted by our calculations, are a direct manifestation of the quantization of the electronic motion in the growth direction of the film. Among possible ways towards an experimental verification of our predictions, the study of the kinetic energy gain of highly charged ions in front of a thin metallic film due to the image charge attraction appears most promising. This energy gain is determined [52,12,34, 53,54] by the set of transition distances corresponding to successive resonant transitions into ionic states with different effective core charges of the ion, i.e., with different principal quantum numbers, and for semi-infinite metal targets has been observed in grazing-incidence experiments. In the case of thin films, the predicted large variation of the transition distances with film thickness suggests that a similar variation occurs in the kinetic energy gain of highly charged ions. A direct observation of this variation is hampered by the fact that well-defined (flat) films exist only at discrete L-values corresponding to integer multiples of the monolayer thickness. However, as the lengths of the L-periodicity intervals in general do not coincide with the monolayer thickness (cf. Figs. 5–7), some experimental evidence can possibly be obtained.

5. Summary and conclusions

We have presented some new theoretical results on the electron dynamics and on resonant level broadening in the interaction of slow atoms and ions with metal surfaces and thin metallic films.

Within the time-dependent close-coupling approach, we have introduced a novel method in which the continuum of metal states is replaced with a finite number of normalizable wave packets. In this way, nondiagonal couplings within the metal subspace, i.e., inelastic one-electron transitions in the conduction band, can be taken into

account. This distinguishes our approach from the time-dependent optical model approach and its fixed-atom (self-energy) limit. To demonstrate the feasibility of the wave-packet method, we have performed an exploratory study of the time evolution of the occupation of hydrogen states in front of a semi-infinite metal. Extensions of this study will have to include the full discretization of the in-plane motion and the detailed examination of one-particle excitation processes and dissipation in the metal.

Our first-order study of resonance broadening of atomic levels near thin metallic films has revealed novel features associated with the size quantization of the electronic motion in the growth direction of the film. The strong variation of the transition distances as a function of film thickness can possibly have observable consequences in the kinetic energy gain of highly charged ions in front of metal surfaces. The evaluation of the full self-energy for atoms interacting with thin metallic films will be a step to be done in the future.

Acknowledgements

This work was supported by NSF Grant PHY-9604872, and by the Division of Chemical Sciences, Office of Basic Energy Sciences, Office of Energy Research, US DOE.

References

[1] H.D. Hagstrum, in: N.H. Tolk, J.C. Tully, W. Heiland, C.W. White (Eds.), Inelastic Ion-Surface Collisions, Academic Press, New York, 1977, p. 1.
[2] H.D. Hagstrum, in: L. Fiermans, J. Vennik, W. Dekeyser (Eds.), Electron and Ion Spectroscopy of Solids, Plenum, New York, 1978, p. 273.
[3] R.A. Baragiola, Radiat. Eff. 61 (1982) 47.
[4] E.W. Thomas, in: S. Datz (Ed.), Applied Atomic Collision Physics, vol. 4. Academic Press, Orlando, 1983, p. 299.
[5] H.D. Hagstrum, in: R. Vanselow, R. Howe (Eds.), Chemistry and Physics of Solid Surfaces VII, Springer, Berlin, 1988, p. 341.
[6] A.T. Amos, K.W. Sulston, S.G. Davison, Adv. Chem. Phys. 76 (1989) 335.
[7] R. Brako, D.M. Newns, Rep. Prog. Phys. 52 (1989) 655.
[8] J. Los, J.J.C. Geerlings, Phys. Rep. 190 (1990) 133.
[9] J. Burgdörfer, in: C.D. Lin (Ed.), Review of Fundamental Processes and Applications of Atoms and Ions, World Scientific, Singapore, 1993, p. 517.
[10] J.W. Rabalais (Ed.), Low Energy Ion–Surface Interactions, Wiley, Chichester, 1994.
[11] H. Shao, D.C. Langreth, P. Nordlander, in: J.W. Rabalais (Ed.), Low Energy Ion–Surface Interactions, Wiley, New York, 1994, p. 117.
[12] A. Arnau, F. Aumayr, P.M. Echenique, M. Grether, W. Heiland, J. Limburg, R. Morgenstern, P. Roncin, S. Schippers, R. Schuch, N. Stolterfoht, P. Varga, T.J.M. Zouros, HP. Winter, Surf. Sci. Rep. 27 (1997) 113.
[13] J. Burgdörfer, E. Kupfer, H. Gabriel, Phys. Rev. A 35 (1987) 4963.
[14] P. Kürpick, U. Thumm, U. Wille, Phys. Rev. A 56 (1997) 543.
[15] P. Kürpick, U. Thumm, Phys. Rev. A 58 (1998) 2174.
[16] A.G. Borisov, D. Teillet-Billy, J.P. Gauyacq, Nucl. Instr. and Meth. B 78 (1993) 49.
[17] G.E. Makhmetov, A.G. Borisov, D. Teillet-Billy, J.P. Gauyacq, Europhys. Lett. 27 (1994) 247.
[18] A.G. Borisov, U. Wille, Surf. Sci. 338 (1995) L875.
[19] A.G. Borisov, U. Wille, Nucl. Instr. and Meth. B 115 (1996) 137.
[20] A.G. Borisov, R. Zimny, D. Teillet-Billy, J.P. Gauyacq, Phys. Rev. A 53 (1996) 2457.
[21] P. Nordlander, J.C. Tully, Phys. Rev. Lett. 61 (1988) 990.
[22] P. Nordlander, J.C. Tully, Phys. Rev. B 42 (1990) 5564.
[23] P. Nordlander, Phys. Rev. B 53 (1996) 4125.
[24] S.A. Deutscher, X. Yang, J. Burgdörfer, Nucl. Instr. and Meth. B 100 (1995) 336.
[25] S.A. Deutscher, X. Yang, J. Burgdörfer, H. Gabriel, Nucl. Instr. and Meth. B 115 (1996) 152.
[26] S.A. Deutscher, X. Yang, J. Burgdörfer, Phys. Rev. A 55 (1997) 466.
[27] F. Martín, M.F. Politis, Surf. Sci. 356 (1996) 247.
[28] P. Nordlander, F.B. Dunning, Phys. Rev. B 53 (1996) 8083.
[29] P. Nordlander, F.B. Dunning, Nucl. Instr. and Meth. B 125 (1997) 300.
[30] J. Hanssen, C.F. Martin, P. Nordlander, Surf. Sci. 423 (1999) L271.
[31] P. Kürpick, U. Thumm, U. Wille, Phys. Rev. A 57 (1998) 1920.
[32] J. Burgdörfer, P. Lerner, F.W. Meyer, Phys. Rev. A 44 (1991) 5674.
[33] J. Burgdörfer, C. Reinhold, F. Meyer, Nucl. Instr. and Meth. B 98 (1995) 415.
[34] J. Ducrée, F. Casali, U. Thumm, Phys. Rev. A 57 (1998) 338.
[35] J. Ducrée, H.J. Andrä, U. Thumm, Phys. Rev. A 60 (1999) 3029.
[36] A.G. Borisov, H. Winter, Nucl. Instr. and Meth. B 115 (1996) 142.
[37] A.G. Borisov, H. Winter, Z. Phys. D 37 (1996) 263.
[38] J.C. Tully, Phys. Rev. B 16 (1977) 4324.
[39] U. Thumm, PhD Thesis, University of Freiburg, 1989.

[40] U. Wille, Phys. Rev. A 45 (1992) 3004.
[41] P. Kürpick, U. Thumm, Phys. Rev. A 54 (1996) 1487.
[42] P.J. Jennings, R.O. Jones, M. Weinert, Phys. Rev. B 37 (1988) 6113.
[43] U. Wille, R. Hippler, Phys. Rep. 132 (1986) 129.
[44] D.F. Gray, Z. Zheng, K.A. Smith, F.B. Dunning, Phys. Rev. A 38 (1988) 1601.
[45] P. Nordlander, F.B. Dunning, private communication.
[46] B. Bahrim, U. Thumm, Bull. Am. Phys. Soc. 44 (1999) 729.
[47] G. Schiwietz, Phys. Rev. A 42 (1990) 296.
[48] G. Bastard, Wave Mechanics Applied to Semiconductor Heterostructures, Les Éditions de Physique, Les Ulis, 1996.
[49] U. Wille, Nucl. Instr. and Meth. B 125 (1997) 310.
[50] U. Wille, Phys. Rev. B 50 (1994) 1888.
[51] U. Thumm, P. Kürpick, U. Wille, Phys. Rev. B 61 (2000) 3067.
[52] H. Winter, J. Phys.: Condens. Matter 8 (1996) 10149.
[53] U. Thumm, Phys. Rev. A 55 (1997) 479.
[54] U. Thumm, Comments At. Mol. Phys. 34 (1999) 119.